Cement and Concrete Composites 134 (2022) 104768

Contents lists available at ScienceDirect

Cement and Concrete Composites

journal homepage: www.elsevier.com/locate/cemconcomp

Ion-adsorption type rare earth tailings for preparation of alkali-based geopolymer with capacity for heavy metals immobilization

Baifa Zhang [a,b,c], Ting Yu [a,c], Liangliang Deng [d], Yun Li [e], Haozhe Guo [f], Junming Zhou [a,c], Lijuan Li [b], Yuan Peng [a,c,g,*]

[a] CAS Key Laboratory of Mineralogy and Metallogeny/Guangdong Provincial Key Laboratory of Mineral Physics and Materials, Guangzhou Institute of Geochemistry, Institutions of Earth Science, Chinese Academy of Sciences, Guangzhou, 510640, China
[b] School of Civil and Transportation Engineering, Guangdong University of Technology, Guangzhou, 510006, China
[c] University of Chinese Academy of Sciences, Beijing, 100049, China
[d] Department of Eco-Engineering, Guangdong Eco-Engineering Polytechnic, Guangzhou, 510520, China
[e] Southern Marine Science and Engineering Guangdong Laboratory (Guangzhou) / Shenzhen Key Laboratory of Natural Gas Hydrates, Academy for Advanced Interdisciplinary Studies, Southern University of Science and Technology, Shenzhen, 518055, China
[f] Institute of Resource Comprehensive Utilization, Guangdong Academy of Sciences, Guangzhou, 510650, China
[g] School of Environmental Science and Engineering, Guangdong University of Technology, Guangzhou, 510006, China

ARTICLE INFO

Keywords:
Mine tailing
Heavy metals
Geopolymer
Immobilization mechanism
Clay minerals

ABSTRACT

Ion-adsorption type rare earth tailings (RET), a type of solid waste that contains clay minerals, were used as a starting material to prepare alkali-based geopolymer. The effects on the compressive strength of RET-based geopolymer, including the modulus and concentration of the alkaline activator, curing temperature, and liquid/solid ratio, were investigated. Pb^{2+} and Cd^{2+} were added during the preparation of the RET-based geopolymer for evaluating the immobilization capacity of heavy metals in the as-obtained geopolymer. The results showed that geopolymer with a compact and dense microstructure was obtained through the optimization of the above factors, with the highest compressive strength being 28.5 MPa. The leaching test indicated that the RET-based geopolymer possessed a desirable capacity for immobilizing heavy metals, where the immobilization efficiency of Pb^{2+} was above 99% and that of Cd^{2+} ranged from 92% to 96%. Heavy metals were immobilized in the RET-based geopolymer matrix through the formation of chemical bonds (T (Si, Al)–O–M (Pb, Cd)) or through an electrostatic attraction between the metal cations and negatively charged $[AlO_4]^-$.

1. Introduction

Geopolymer is a type of polymeric cementitious material that exhibits excellent properties, such as high compressive strength [1], low thermal conductivity [2], and suitable chemical resistance [3]. So far, geopolymer has been regarded as a promising alternative to ordinary Portland cement (OPC) because of its less environmental footprint (e.g., less CO_2 emission, lower energy-consuming, etc.) [4] and better properties. Owing to its three-dimensional network structure, geopolymer also acts as an excellent binder that can firmly immobilize heavy metals, such as Pb^{2+}, Cd^{2+}, Cr^{6+}, and Zn^{2+} [5,6], and exhibits improved durability and compatibility with heavy metals over OPC [7–10]. For example, Demir and Derun [11] used gold mine tailings for preparing geopolymer, which exhibited a high capacity for Pb adsorption, with an adsorption efficiency of 94%. Normally, a geopolymer is synthesized by activating aluminosilicates with a high concentration of alkaline solution [12]. It's worthwhile to note that aluminosilicates with sufficient amounts of reactive alumina and silica can be used as geopolymer precursors [13–15]. This means that many solid wastes, such as fly ash [16], slag [17], sludge [18], and mine tailing [19], can be used for geopolymer preparation, which is a promising way to recycle wastes.

Rare earth elements, especially middle and heavy rare earth elements, are important materials with wide application to electronics, healthcare, and other high-tech industries [20,21]. Ion-adsorption type rare earth (IRE) ores form the most important heavy rare earth resource, which provides most of the heavy rare earths consumed annually worldwide. The rare earths in these deposits mainly occur as (hydrated) cations adsorbed on the surface of clay minerals (e.g., kaolinite,

* Corresponding author. Key Laboratory of Mineralogy and Metallogeny, Guangzhou Institute of Geochemistry, Institutions of Earth Science, Chinese Academy of Sciences, Wushan, Guangzhou, 510640, China.
E-mail address: yuanpeng@gig.ac.cn (Y. Peng).

https://doi.org/10.1016/j.cemconcomp.2022.104768
Received 17 April 2022; Received in revised form 27 August 2022; Accepted 11 September 2022
Available online 15 September 2022

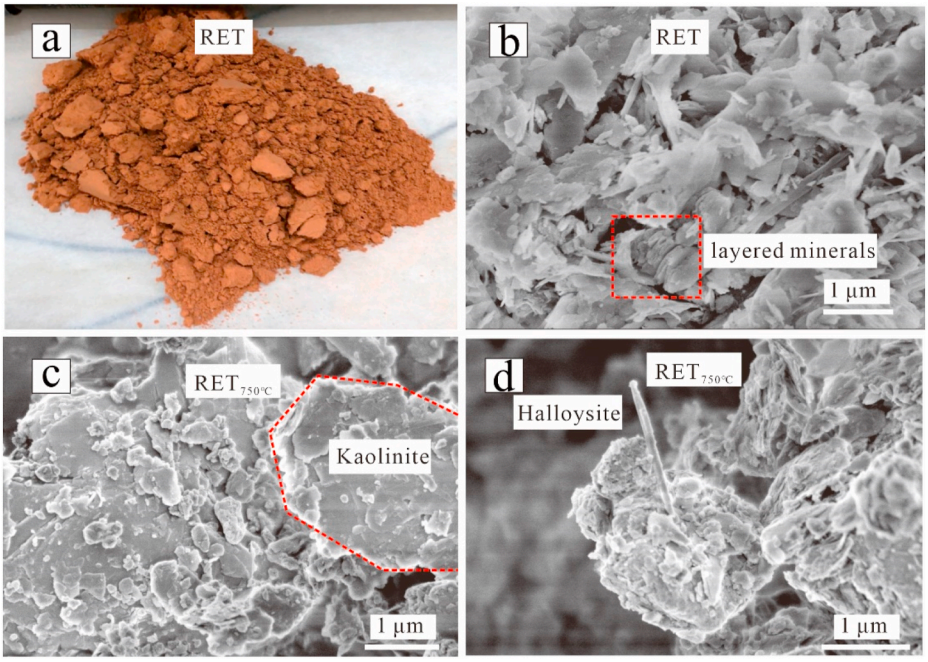

Fig. 1. (a) photograph and (b) SEM image of RET; (c) and (d) SEM images of $RET_{750°C}$.

halloysite, and illite) [22,23]. However, owing to their low grade (containing 0.05–0.2 wt%, RE_2O_3) [24], considerable rare earth tailings (RETs) are produced after the extraction process. It is estimated that 2000 tons of RETs are disposed into adjacent valleys or streams for the production of 1 ton of rare earth oxide and that China produces 60,000 tons of rare earth concentrate annually [25,26]. The accumulation of considerable RET exerts a detrimental effect on the environment and ecology [27]. In addition, RETs often contain heavy metals (e.g., Pb^{2+}, Cd^{2+}, and Cu^{2+}), whose the migration during rains can lead to heavy metal pollution in soil and water [28], which has serious health hazards for humans. Therefore, a feasible approach of reusing RET for environmental, social, and economic benefits is urgently required.

As mentioned above, IRE ores contain considerable clay minerals [29], which account for 40%–70% of all minerals present in IRE ores. Exchangeable rare earth ions can be easily extracted using an electrolyte solution, but the mineral component remains unchanged, indicating that RET still contain considerable clay minerals [25]. Therefore, how to take full advantage of the clay minerals present in RET is the key to reusing and recycling RET. Furthermore, during reutilization, the toxicity of the heavy metals present in RET must be reduced. Cement immobilization has been widely used to convert heavy metals into an environmentally acceptable form [8,30]. However, its disadvantages, including high CO_2 emission, permeability, and leaching concentration make it unable to meet the increased demand for environmental protection and limit its wide application [8].

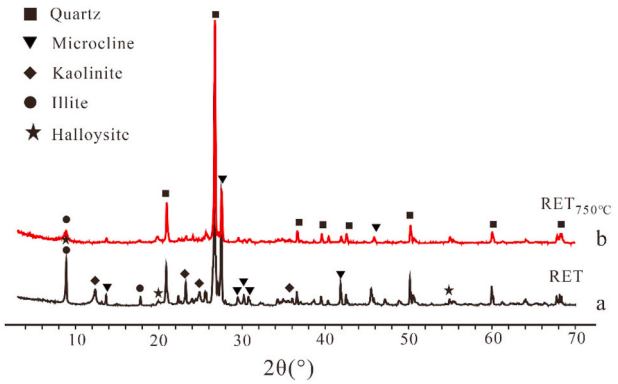

Fig. 2. X-ray diffraction patterns of (a) rare earth tailing and (b) its calcination product.

According to the mineralogical analysis, RET may exhibit potential geopolymerization reactivity because they contain many clay minerals [31,32]. Therefore, alkali activation of RET for preparing high-performance geopolymers is an interesting issue that merits investigation. Particularly, as mentioned above, heavy metals can be effectively immobilized during geopolymerization simultaneously, which can reduce the biotoxicity of RET. Therefore, geopolymerization via alkali activation may be a promising technology for a comprehensive utilization of such RET. Despite that, RET-based geopolymer has rarely been studied. A recent study conducted by Hu et al. [33] utilized RET (obtained from Western Sichuan Province, China) to prepare geopolymer for immobilization of Pb^{2+} and Ba^{2+}. However, they focused on the effect of the addition of calcined kaolinite on the mechanical properties of RET-based geopolymer because the RET they used was bastnaesite type (mainly containing veatchite, collinsite, and phlogopite) that showed rather low reactivity.

In this study, the feasibility of directly using ion-adsorption type RET for preparing alkali-activated geopolymer was assessed. The effects of curing temperature, concentration and modulus of sodium silicate, and liquid/solid ratio on the compressive strength of the obtained geopolymer were investigated. Given that Pb^{2+} and Cd^{2+} commonly exist in RETs and can be readily migrated [34,35], they are added into the RET-based geopolymers for evaluating their immobilization capacity. To analyze the performance of the RET-based geopolymer and its immobilization mechanism, the compressive strength of the geopolymers and leaching concentration of the heavy metals are tested, followed by the application of various characterization methods. Finally, the immobilization mechanisms of the heavy metals for RET-based geopolymer are discussed.

2. Experimental

2.1. Materials

Ion-adsorption type rare earth tailings (RET) were obtained from a rare earth processing plant in Jiangxi Province, China, with the

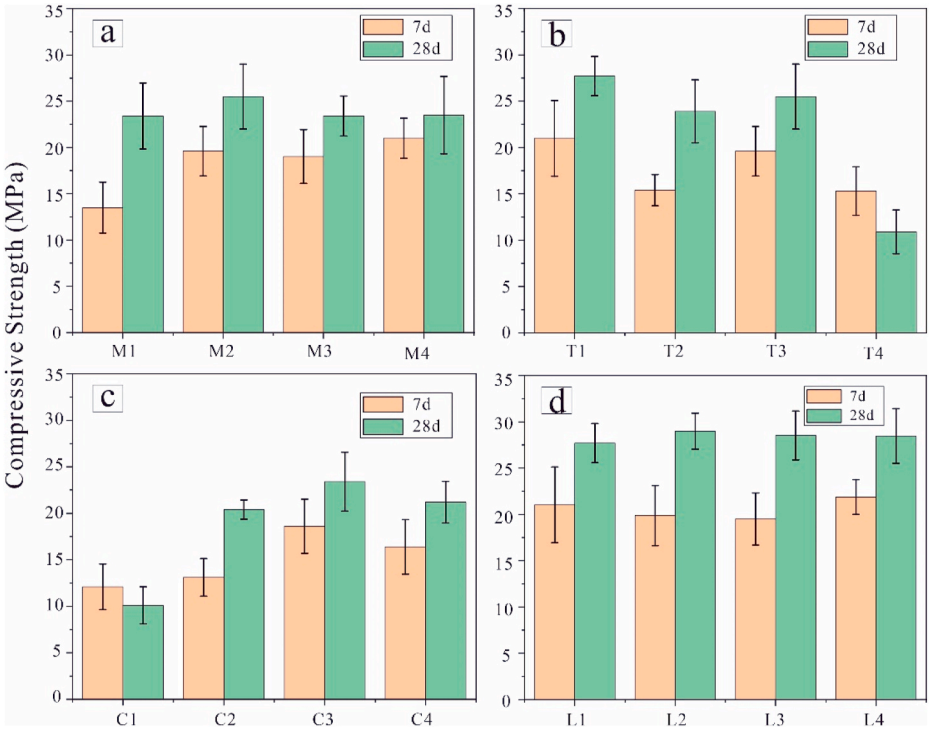

Fig. 3. Effects of different factors on compressive strengths of geopolymer. (a) Modulus of sodium silicate, (b) curing temperature, (c) concentration of sodium silicate, (d) liquid/solid ratio.

following chemical composition (wt%): SiO_2 (68.45%), Al_2O_3 (14.38%), Fe_2O_3 (5.86%), K_2O (3.21%), Na_2O (0.22%), MgO (0.81%), CaO (0.04%), Ti_2O (1.17%), SrO_2 (<0.01%), Li_2O (0.010%), PbO (<0.01%), ZnO (<0.01%), Rb_2O (0.013%), SO_3 (<0.01%), ZrO_2 (0.013%), MnO (0.052%), B_2O_3 (<0.01%), P_2O_5 (<0.01%), and loss on ignition (5.66%). The RET were ground using a ball mill for 4 h, and then passed through an 80-mesh (200 μm) sieve. The powdered RET exhibited a greyish red color and looked like earthy (Fig. 1a). Finally, the powder was calcined in a muffle furnace at 750 °C in air for 2 h (heating/cooling rate: 5 °C/min), and denoted as $RET_{750°C}$.

Fig. 1b shows that besides minerals with irregular shape, there were many layered minerals in RET, which should be attributed to clay minerals. Fig. 2a also evidences that the RET contained clay minerals, such as kaolinite, halloysite, and illite. Meanwhile, quartz and microcline were also found.

After calcination at 750 °C, the quartz remained intact due to its high thermal stability (Fig. 2b). In contrast, the X-ray diffraction (XRD) reflections attributed to kaolinite, halloysite, and illite disappeared and the intensity of the microcline and illite reflections reduced, which indicated that these minerals were completely or partly transformed into the amorphous phase. However, kaolinite and halloysite can keep their original morphologies after calcination. Thus, hexagonal plates of kaolinite (Fig. 1c) and nanotubular halloysite (Fig. 1d) can be found in $RET_{750°C}$.

Alkaline solutions were prepared by mixing commercial sodium silicate (Na_2O 8.5 wt%, SiO_2 26.5 wt%, H_2O 65.0 wt%) with chemical grade NaOH pellets (purity ≥96%). Ultrapure water was added to adjust the concentration of the solution, which was then stored for 24 h before use. The heavy metals—Pb^{2+} and Cd^{2+}, in the forms of $Pb(NO_3)_2$ and $Cd(NO_3)_2•4H_2O$ (purity ≥96%)—were obtained from commercial suppliers.

2.2. Preparation of geopolymer with and without addition of heavy metals

$RET_{750°C}$ was mixed with the alkaline solution to form a homogeneous paste, and then cast into silica molds (20 × 20 × 20 mm^3). To prevent water evaporation, the molds were covered with a thin polyethylene film and the moulded specimens were cured at different temperatures for 48 h. Then, the specimens were removed from the molds and stored in plastic bags at ambient temperature until the day of the test. The detailed experimental conditions are detailed in Table S1.

The contents of the heavy metals (Pb^{2+}, Cd^{2+}, and a combination of both) accounting for the total mass of the RET were set to 0.5, 1.0, and 1.5 wt%. The mix proportion of raw materials for salt-containing RET-based geopolymer was set to same as the L3 in Table S1. The corresponding content of salts ($Pb(NO_3)_2$ and $Cd(NO_3)_2•4H_2O$) were dissolved into a part of the free ultrapure water to form solutions firstly, and sodium silicate with a modulus of 1.0 was separately dissolved in the rest of the water. The heavy metal-containing saline solution was homogeneously mixed with $RET_{750°C}$ for 5 min. Then, sodium silicate was added and mixed to form a homogeneous paste with a liquid/solid ratio of 0.4. The paste was cast into silicon molds (20 × 20 × 20 mm^3) and cured at ambient temperature for 28 days. The obtained products were labeled as GMT-aM, where "a" represents the mass ratio and "M" represents the heavy metal. For example, GMT-0.5 Pb indicates geopolymer with an addition of 0.5% Pb^{2+}.

2.3. Leaching test for the geopolymers with addition of heavy metals

A leaching test was conducted to analyze the immobilization efficiency of the heavy metals. The geopolymers with the addition of different heavy metals were first crushed, and then passed through a 10-mesh (2.0 mm) sieve. Next, 2.0 g of the geopolymer powder was mixed with 40 mL of acetic acid solution (pH 2.88 ± 0.05) in a polyethylene container, and added to a shaker for 20 h (25 ± 2 °C, 100 rpm). The resulting mixture was then centrifuged at a speed of 10,000 rpm, and the supernatant was passed through a 0.48-μm filter. The concentrations of Pb^{2+} and Cd^{2+} in the solution were determined using an iCAP 7000 series inductively coupled plasma optical emission spectrometer (Thermo Scientific, USA). The geopolymers after the leaching test were labeled as GMT-aM-F.

2.4. Characterization methods

The 7 and 28 d compressive strengths of geopolymers prepared by different conditions were test using YAW-300D Compression Resistance Tester. The loading rate was 0.5 N/s.

The powder XRD patterns of geopolymers were recorded on a Bruker D8 Advance diffractometer with Ni filter and CuKα radiation using a generator voltage of 40 kV, a generator current of 40 mA, and a scanning speed of 3°/min. The FTIR spectra of geopolymers were recorded on a Bruker Vertex 70 spectrometer with a resolution of 4 cm^{-1} with 64 scans in the range of 4000–400 cm^{-1}. The XPS spectra of geopolymers were performed on a K-Alpha XPS instrument. The Al Kα source (1486.8 eV) was operated at an emission current of 3 mA and a tube voltage of 12 kV. The solid-state ^{27}Al MAS NMR spectra and ^{29}Si CP/MAS NMR spectra of geopolymers were recorded on a Bruker Avance III 600 spectrometer with a magnetic field strength of 14.1 T. For ^{27}Al MAS NMR spectra, the resonance frequency was 156.4 MHz, the small-flip angle technique with a pulse length was 0.5 μs (<π/12), the recycle delay was 1 s, and the spinning rate was 14 kHz. For ^{29}Si MAS NMR spectra, the resonance frequency was 119.2 MHz, the contact time was 6 ms, the π/2 pulse length was 2.3 μs, the recycle delay was 2 s, and the spinning rate was 10 kHz. The chemical shifts of ^{27}Al and ^{29}Si were given in ppm referenced to 1 mol/L $Al(NO_3)_3$ and tetra-methylsilane (TMS), respectively.

SEM observation of geopolymers was performed using an SU8010 field-emission scanning electron microscope with an accelerating voltage of 15 kV and a current of 10 mA. The sputtering of gold (Au) was carried out to make an ultra-thin electrically conducting coating before FE-SEM observation. The chemical compositions of geopolymers were obtained through energy-dispersive X-ray (EDX) spectroscopy. TEM images and EDX spectroscopy of geopolymers were collected on an FEI Talos F200S field-emission, which is operating at an accelerating voltage of 200 kV.

3. Results and discussion

3.1. Compressive strength of RET-based geopolymers

Fig. 3 shows the compressive strengths of RET-based geopolymer prepared under different conditions. The optimal sodium silicate modulus highly depends on the properties of aluminosilicates [36,37]. As shown in Fig. 3a, the 28-day compressive strength of RET-based geopolymers was highest when using the alkali activator with a modulus of 1.0 (M2). When the sodium silicate modulus was below 1.0, the excess alkali content caused the efflorescence and brittleness of the RET-based geopolymer [38]. In contrast, when the sodium silicate modulus exceeded 1.0, the low alkalinity of the solution insufficiently dissolved the $RET_{750°C}$ and the polycondensation of the labile species was inhibited due to the high polymerization degree of the silicate [39]. Consequently, the 28-day compressive strength increased as the modulus was increased to 1.0 and slightly decreased as the modulus was further increased.

As shown in Fig. 3b, the RET-based geopolymer cured at ambient temperature exhibited the highest compressive strength (T1). When the curing temperature was increased, the compressive strength reduced slightly. The optimal curing temperature varied for different aluminosilicate precursors [40,41]. For alkali activation of $RET_{750°C}$, increasing the curing temperature led to a rapid setting and hardening of the geopolymer without sufficient dissolution, which decreased the geopolymerization degree. Moreover, the higher curing temperature produced a geopolymer with more porous structure due to more rapid evaporation of water. Therefore, curing at ambient temperature not only improved the compressive strength but also reduced the energy input required for preparing the RET-based geopolymer.

The first step of geopolymerization involved the dissolution of aluminosilicate, which was strongly affected by the concentration of the alkaline solution [42,43]. The 28-day compressive strength of the RET-based geopolymer increased from approximately 10 (C1) to 24 MPa (C3) when the concentration was increased from 25% to 35%, because a more soluble Si and higher alkalinity improved the degree of geopolymerization [44,45]. Therefore, an increased geopolymerization resulted in better performance of the as-obtained geopolymer. However, when the concentration was increased to 40%, the alkaline solution became highly viscous and the workability of the geopolymeric paste reduced due to the lower water content [46,47], which might have inhibited the dissolution of $RET_{750°C}$. Meanwhile, the geopolymeric gel tended to be precipitated prematurely, which slightly decreased its compressive strength [47].

The mechanical properties of the alkali activation of $RET_{750°C}$ were controlled by the liquid/solid ratio. Increasing this value increased the workability of the geopolymeric paste and accelerated the dissolution of aluminosilicates, which in turn increased the early compressive strength of the as-obtained geopolymer [48]. However, a high liquid/solid ratio also indicated the presence of excess water, which decreased the polycondensation of the aluminosilicates and generated more pores during curing, thus reducing the late compressive strength [45]. Therefore, the 28-day compressive strength (28.5 MPa) did not change substantially as the liquid/solid ratio was increased from 0.34 (L1) to 0.43 (L3), possibly because the adverse and favorable effects canceled each other out in this range for the alkali activation of $RET_{750°C}$.

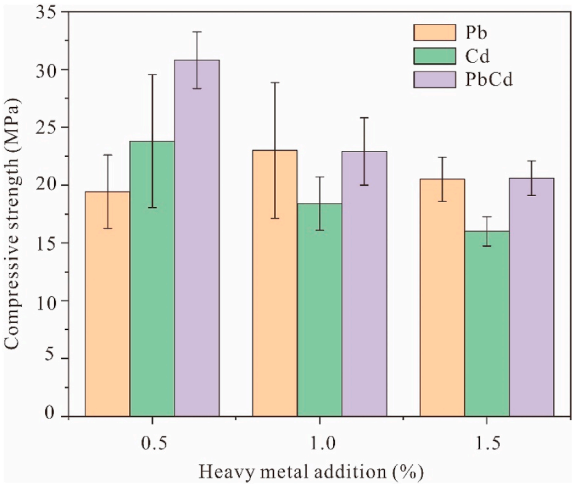

Fig. 4. The 28-day compressive strengths of geopolymers with addition of heavy metals.

3.2. Heavy metal immobilization in RET-based geopolymer

3.2.1. Effect of heavy metals on compressive strength of RET-based geopolymer

The 28-day compressive strengths of RET-based geopolymers with the addition of heavy metals are shown in Fig. 4. The addition of heavy metals (except GMT-0.5PbCd) reduced the compressive strengths of the geopolymer, which has also been observed in previous studies conducted on fly ash-based geopolymers [5,49]. The addition of heavy metals during geopolymerization not only reduced the alkalinity of solution but also hindered the polymerization of $[SiO_4]$ and $[AlO_4]$ [8]. Therefore, the reduced geopolymerization degree resulted in low compressive strength of the geopolymers. However, the compressive strength of GMT-0.5PbCd slightly increased, indicating that the effect of heavy metal addition was dependent on the identity of the metals. As the concentrations of Cd^{2+} and Pb^{2+}+Cd^{2+} were increased from 0.5% to 1.5%, the geopolymers' compressive strengths decreased from 23.8 to 16.3 MPa and from 31.0 to 20.6 MPa, respectively. Thus, greater amounts of heavy metals had a more negative impact on the mechanical properties than did smaller amounts [8].

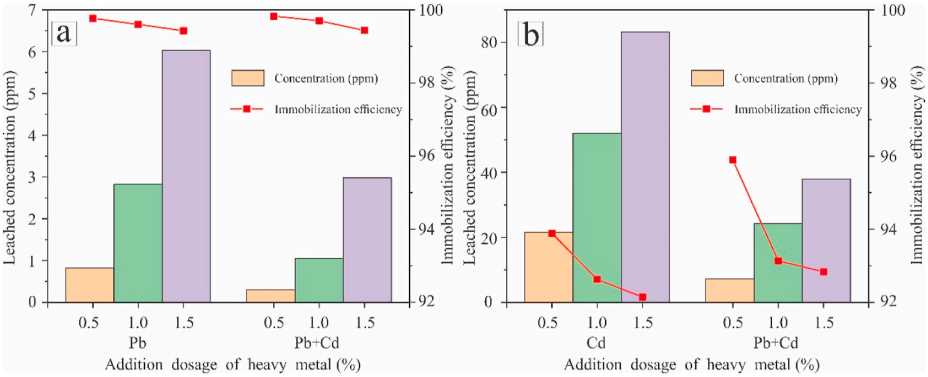

Fig. 5. Leached concentration and immobilization efficiency of (a) Pb^{2+} and (b) Cd^{2+} added to RET-based geopolymers.

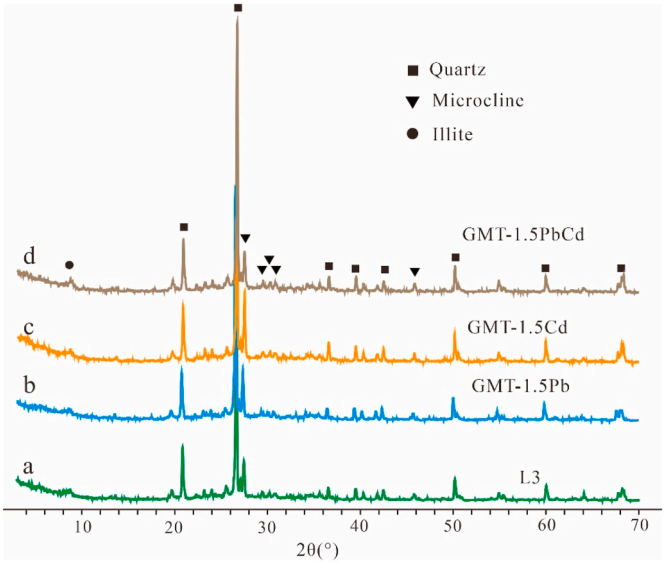

Fig. 6. X-ray diffraction patterns of geopolymers with and without the addition of heavy metals: (a) L3, (b) GMT-1.5 Pb, (c) GMT-1.5Cd, and (d) GMT-1.5PbCd.

These results demonstrate that the different heavy metals had different impacts on the mechanical properties of the geopolymers, which is complicated and warrants further study. The compressive strengths of all RET-based geopolymer exceeded 15 MPa even after the addition of heavy metals; thus, these materials can be applied as construction materials [50].

3.2.2. *Immobilization of heavy metals in RET-based geopolymer*

The leaching concentration and immobilization efficiency of the heavy metals added to the RET-based geopolymer are displayed in Fig. 5, where the leached heavy metal concentration increased with the amount of additive. The leached Pb^{2+} concentration increased from 0.30 to 6.03 ppm and the leached Cd^{2+} concentration increased from 4.11 to 83.24 ppm.

As the additive amounts of the heavy metals were increased, the immobilization efficiency of Pb^{2+} and Cd^{2+} decreased. The immobilization efficiency of Pb^{2+} was higher than 99%, whereas that of Cd^{2+} was lower than 96%, which indicated that the immobilization effect varied with different heavy metals. This result can be attributed to the different properties of the heavy metals. On one hand, the number of moles of Pb is less than that of Cd under the same addition dosage by weight, because the atomic mass of Pb is greater than that of Cd. Therefore, the geopolymer must provide more solidification sites for Cd than Pb if the immobilization efficiency is at the same level. On the other hand, Pb^{2+} has a larger ion size than Cd^{2+}, which facilitates the formation of larger

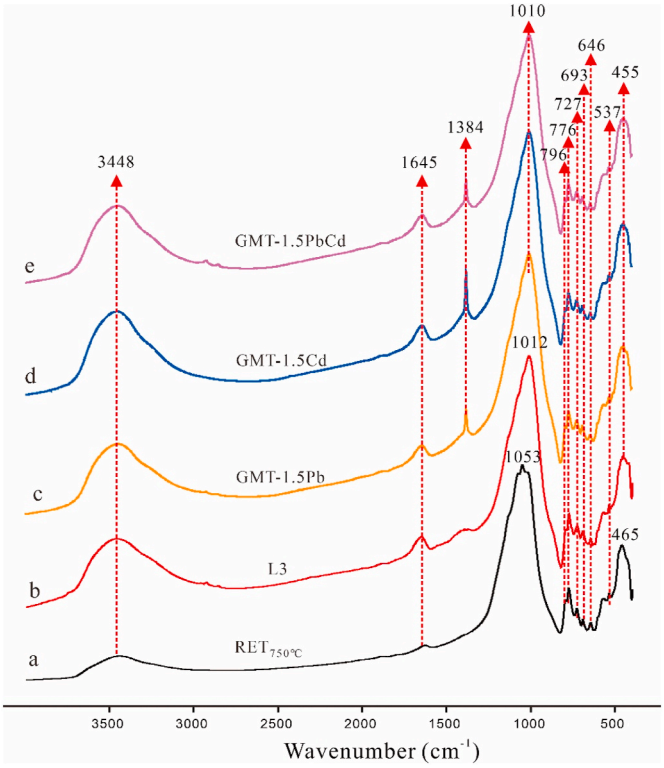

Fig. 7. Fourier-transform infrared spectra of calcined rare earth tailings-based geopolymer with and without the addition of heavy metals: (a) $RET_{750°C}$, (b) L3, (c) GMT-1.5 Pb, (d) GMT-1.5Cd, and (e) GMT-1.5PbCd.

aluminosilicate oligomers, and thus, Pb^{2+} can be more effectively immobilized in the geopolymer matrix [51,52]. Moreover, the large ionic radius of Pb^{2+} reduces its mobility compared with Cd^{2+} [53]. Therefore, the immobilization efficiency of Pb^{2+} was higher than that of Cd^{2+}. Note that irrespective of the number of metal elements added to the geopolymer, similar immobilization efficiency was achieved, indicating that different heavy metals had little interaction during immobilization in RET-based geopolymer.

3.3. *Structure of RET-based geopolymer with/without addition of heavy metals*

3.3.1. *X-ray diffraction (XRD) results*

Fig. 6 shows the XRD patterns of RET-based geopolymer with and without the addition of 1.5% heavy metals. As shown in Fig. 6a, the quartz and microcline remained intact after geopolymerization due to

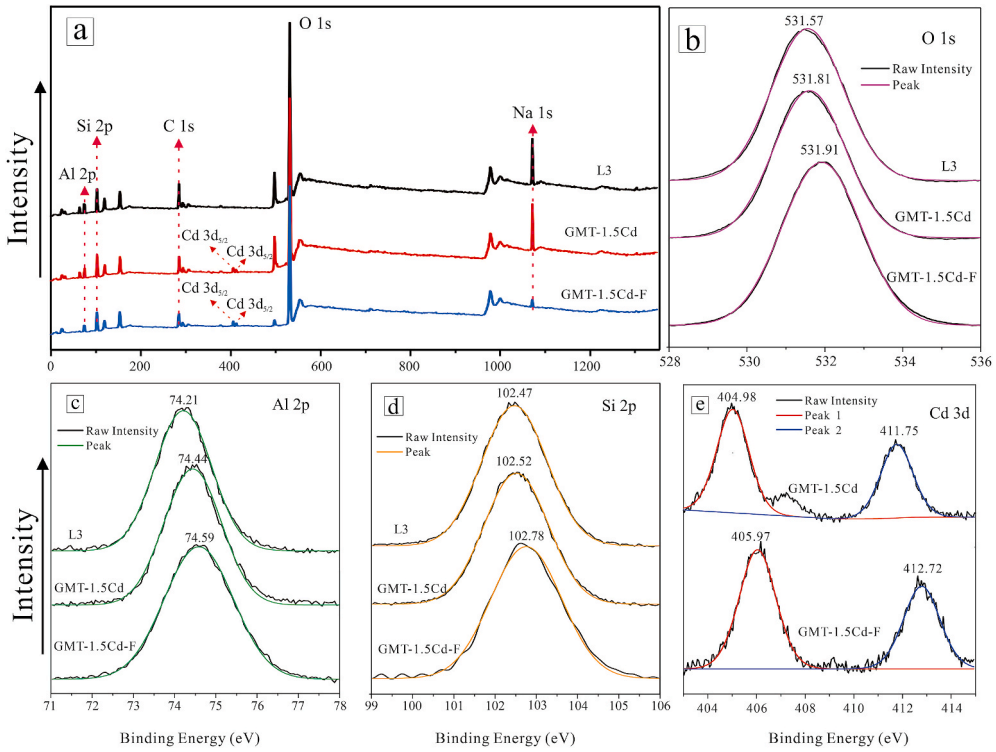

Fig. 8. X-ray photoelectron spectra of geopolymers with and without the addition of 1.5% Cd: (a) wide-scan results, (b) O 1s, (c) Al 2p, (d) Si 2p, and (e) Cd 3d

their high chemical stability. The typical broad reflection around 20° (2θ)–35°(2θ), related to the formation of amorphous geopolymer, is not pronounced in Fig. 5a, which is attributable to the presence of many unreacted minerals.

Notably, there was no obvious difference among the geopolymers in terms of diffraction patterns after the addition of heavy metals. This result demonstrates that no new crystalline phase containing Pb or Cd was formed during the geopolymerization. According to Wan et al. [54], Pb^{2+} is mainly incorporated in silicate glass or in the network, instead of the crystal. Therefore, the addition of 1.5% Pb^{2+} or Cd^{2+} did not substantially change the mineral phases of the geopolymer.

3.3.2. *Fourier-transform infrared (FTIR) results*

The FTIR spectra of $RET_{750°C}$, RET-based geopolymers, and the geopolymers with the addition of 1.5% heavy metals are shown in Fig. 7. In the FTIR spectrum of $RET_{750°C}$, the broad peak at 3448 cm^{-1} was attributed to the stretching vibration of O–H, while the peak at approximately 1645 cm^{-1} was attributed to the bending vibration of O–H from the physically adsorbed H_2O [41]. The main band at 1053 cm^{-1} was attributed to the Si–O–Si stretching vibration of the clay minerals (e.g., kaolinite and halloysite). The absorption peaks of 796, 776, and 693 cm^{-1} were also attributed to the symmetric stretching vibration of Si–O–T (T: Al or Si) originating from the clay minerals in $RET_{750°C}$ [55], whereas the bands at 535 and 465 cm^{-1} were attributed to Al–O–Si and Si–O–Si deformation vibrations, respectively. The peaks at both 727 and 646 cm^{-1} corresponded to the Si–O stretching vibration, and were attributed to microcline and kaolinite, respectively [56].

After the alkali activation of $RET_{750°C}$, the main band with a wavenumber of 1053 cm^{-1} shifted to a lower wavenumber of 1012 cm^{-1}, which indicated the formation of a geopolymer, i.e., the partially dissolved $RET_{750°C}$ reorganized to form Si–O–T bonds. However, other typical vibrations of Si–O–T (776, 727, and 693 cm^{-1}) originating from the geopolymer were overlapped by those originating from the unreacted minerals, and it was difficult to distinguish the Si–O–T vibrations between the unreacted minerals and RET-based geopolymers [57]. Furthermore, the FTIR spectrum of L3 was similar to those of GMT-1.5Pb, GMT-1.5Cd, and GMT-1.5PbCd, which confirmed that the addition of heavy metals did not substantially alter the structure of the RET-based geopolymer.

A new peak at approximately 1384 cm^{-1} appeared in the FTIR spectra of the heavy metal-containing geopolymers. Some studies have attributed this peak to the presence of excess SiO_3^{2-} or CO_3^{2-} [58–60]. However, considering the absence of this peak in the L3 sample, this absorption should be assigned to the stretching vibration of NO_3^- originating from $Pb(NO_3)_2$ and $Cd(NO_3)_2$ [57]. Meanwhile, the asymmetric stretching vibration of Si–O–T at 1012 cm^{-1} in L3 (Fig. 7a) shifted to a lower wavenumber (Fig. 6b–d) after the addition of heavy metals. This might be because the replacement of Na^+ with Pb^{2+} or Cd^{2+} slightly affected the Si–O–Al vibration resulting from the formation of a complex cation around $[AlO_4]^-$ [58]. However, Wan et al. [10] determined that the addition of 6% $Pb(NO)_3$ during geopolymerization did not alter the geopolymer formation.

3.3.3. *X-ray photoelectron spectroscopy (XPS) results*

Fig. 8a shows the XPS wide-scan results of L3, GMT-1.5Cd, and GMT-1.5Cd–F. The Na, Si, Al, and O elements were detected in all samples. Meanwhile, the observation of Cd in the XPS spectrum of GMT-1.5Cd indicated that Cd^{2+} was effectively incorporated in the geopolymer matrix. After the leaching process, Cd^{2+} could still be detected from GMT-1.5Cd–F, demonstrating that Cd^{2+} was successfully immobilized in the RET-based geopolymer.

Fig. 8b–d displays the XPS narrow-scan results. After the addition of Cd^{2+} during geopolymerization, the binding energies of Si 2p, Al 2p, and O 1s slightly increased from 102.47 to 102.52 eV, 74.21–74.43 eV, and 531.57–531.81 eV, respectively. These results agreed with those obtained by Guo and Huang [61], who reported that the binding energies of Si 2p, Al 2p, and O 1s geopolymers increased after the addition of heavy metals. This is attributable to the formation of a Si–O–Cd or Al–O–Cd bond [6,62]. As is well-known, the binding energy of an element results from the strong Coulomb interaction between electrons and the nucleus, which is influenced by the shielding effect of the outer electrons. Due to the reaction between $T–O^-$ and Cd^{2+} (or Cd complex),

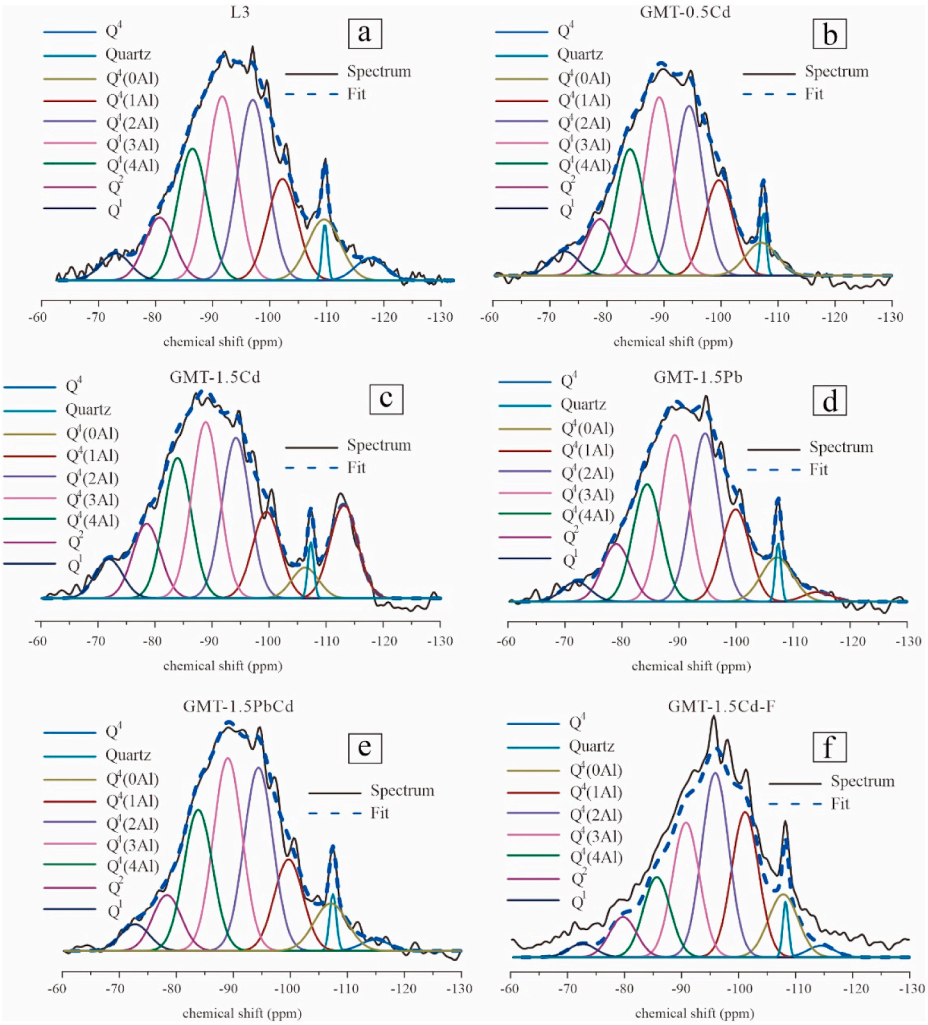

Fig. 9. Deconvolution results obtained for ^{29}Si cross-polarization/magic-angle spinning nuclear magnetic resonance spectra of RET-based geopolymers with and without the addition of heavy metals: (a) L3, (b) GMT-0.5Cd, (c) GMT-1.5Cd, (d) GMT-1.5 Pb, (e) GMT-1.5PbCd, and (f) GMT-1.5Cd–F.

the electron cloud density of Si, Al, and O elements decreases, leading to increased binding energy [63]. Particularly, compared with Si 2p and O 1s, the change in Al 2p is more significant, which is attributable to the fact that the partial Cd^{2+} replaces the Na^{+} around the $[AlO_4]^{-}$ tetrahedron, affecting the binding energy of Al 2p [6]. After the leaching test, the binding energies of Si 2p, Al 2p, and O 1s further increased to 102.78, 74.58, and 531.91 eV, respectively. In the acid medium, the aluminosilicate bonding of the geopolymer was broken, followed by the formation of Si–OH and Al–OH [64]. H^{+} exhibited higher electron-accepting capacity than Na^{+} or Cd^{2+}, leading to an increase in the binding energy.

Fig. 8e shows that, in the XPS results of Cd 3d, there are two peaks at approximately 404.98 and 411.77 eV, which are expected to be related to Cd $3d_{5/2}$ and Cd $3d_{3/2}$, respectively. This result indicates that Cd^{2+} was incorporated in the geopolymer in a divalent state [65]. Combining the XPS results of Pb and Cd in GMT-1.5 Pb and GMT-1.5PbCd (Fig. S1), it can be concluded that geopolymerization did not alter the chemical valence states of the heavy metals. After leaching, the binding energy of Cd 3d increased. This phenomenon implies that a part of the immobilized Cd leached out from the geopolymer, the amount of Cd within close range of O and Al decreased, and the shielding effect thus decreased, which increased the binding energy of Cd 3d. Similar results were obtained for the GMT-1.5 Pb and GMT-1.5PbCd samples (Fig. S1).

3.3.4. Nuclear magnetic resonance (NMR) results

Fig. S2 shows the ^{27}Al NMR magic-angle spinning (MAS) and ^{29}Si cross-polarization (CP)/MAS NMR spectra of the RET-based geopolymers. The ^{27}Al NMR MAS spectrum (Fig. S2a) exhibited a strong resonance centered at 57 ppm, which was attributed to the four-coordinate Al (Al^{IV}) of the alkali-based geopolymer. In addition, a small resonance centered at 3 ppm was attributed to the six-coordinate Al (Al^{VI}), suggesting that some unreacted minerals remained in the RET-based geopolymer. After the addition of heavy metals, the intensity of the resonance at approximately 57 ppm increased and the chemical shift changed, but by an amount too slight to quantify. This result was supported by Walkley et al. [66], who concluded that the peak attributed to Al^{IV} became narrow and more intense after the incorporation of Sr and Ca into a geopolymer, due to the reduction of the Al/Si ratio. However, Ji and Pei [6] reported that the addition of heavy metals substantially altered the chemical shift and intensity. These different results are attributable to the different contents of the heavy metals, where the low content of heavy metal used in this study did not substantially alter the local structure of the Al environment in the geopolymer framework. After leaching, the intensity of the resonance at approximately 57 ppm decreased, accompanied with an increase in the content of Al^{VI}.

In Fig. S2b, the ^{29}Si CP/MAS NMR spectra of all RET-based geopolymers show a broad resonance ranging from −70 to −120 ppm due to the poorly ordered structure of the aluminosilicate [67]. This broad peak is attributable to the overlapping resonances resulting from different Si

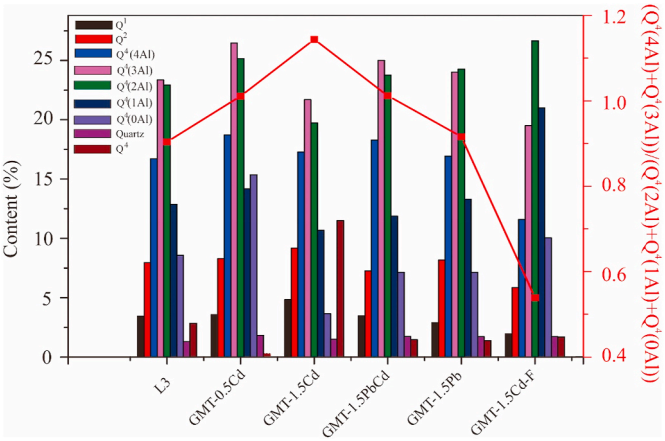

Fig. 10. Normalized summary of Q^4(mAl) Si coordination environments in RET-based geopolymer identified in the deconvoluted ^{29}Si cross-polarization/magic-angle spinning nuclear magnetic resonance spectra.

environments, including the Si environments of the newly formed geopolymer and the unreacted raw materials [68]. Hence, Gaussian peak deconvolution was conducted to enhance the low spectral resolution of the ^{29}Si CP/MAS NMR spectra. Nine peaks were observed after the deconvolution (Fig. 9), and Fig. 10 presents the fractional areas of the constituent peaks.

For the ^{29}Si CP/MAS NMR spectrum of L3 (Fig. 9a), the broad peaks at approximately −72 and −79 ppm were attributed to the less-condensed Si species (Q^1 and Q^2). Meanwhile, a small and broad peak at approximately −115 ppm was assigned to the polymerized silica (Q^4). A sharp peak appearing at −107 ppm indicated the presence of quartz [69]. The content of these Si species slightly increased after the addition of heavy metals, indicating that less Si was incorporated in the geopolymer matrix. Therefore, the compressive strength of the geopolymer tended to decline.

Furthermore, the five peaks at approximately −107, −100, −95, −89, and −84 ppm were assigned to Q^4(0Al), Q^4(1Al), Q^4(2Al), Q^4(3Al), and Q^4(4Al), respectively. These peaks were attributed to the different Si environments of an amorphous geopolymer. The addition of Cd^{2+} evidently altered the composition of the RET-based geopolymers, increasing the fraction of Q^4(mAl) structural units rich in Al (i.e., Q^4(3Al) and Q^4(4Al)) (Fig. 10). As the amount of Cd^{2+} added was increased, the value of $(Q^4(4Al)+Q^4(3Al))/(Q^4(0Al)+Q^4(1Al)+Q^4(2Al))$ increased, demonstrating that more Al was incorporated in the geopolymer matrix. This may be because when monovalent cations are substituted by divalent cations, the charge-balancing capacity of geopolymer increases [66]. In contrast, the addition of 1.5% Pb^{2+} did not substantially alter the fraction of Q^4(mAl) structural units. However, Nikolić et al. reported that the addition of 4% Pb or 2% Cr increased the fraction of Q^4(mAl) structural units rich in Si (i.e., Q^4(0Al), Q^4(1Al), and Q^4(2Al)) [67,70]. This difference can be attributed to the varied contents of Pb^{2+}. In this study, the content of Pb^{2+} added to the geopolymer was low, so it might have had a lesser impact on the composition of the RET-based geopolymer. The abovementioned results indicate that the addition of heavy metals affected the composition of the as-obtained geopolymers, which eventually affected their mechanical properties.

Table 1
The EDX results of geopolymers.

spot	Elements (%, atomic ratio)							
	Si	Al	Cd	Pb	O	Na	Fe	Mg
#1	14.1	10.5	–	–	67.5	5.0	1.4	1.5
#2	19.3	10.5	–	–	59.3	10.9	–	–
#3	16.1	7.8	–	0.2	68.9	7.1	–	–
#4	18.7	9.9	–	0.2	63.1	8.1	–	–
#5	17.6	8.2	0.2	–	69.5	4.5	–	–
#6	16.2	9.3	0.5	–	63.0	9.5	–	–
#7	18.1	9.5	0.3	0.2	60.2	10.7	–	–
#8	20.8	13.6	0.2	0.1	62.0	3.3	–	–

After leaching, the contents of Q^4(0Al), Q^4(1Al), and Q^4(2Al) increased substantially, accompanied with a decrease in the contents of Q^4(3Al) and Q^4(4Al). This result demonstrates that the geopolymer structure was destroyed, leading to the depolymerization of the geopolymer and increase in the concentration of Si-rich species.

3.4. Morphology of RET-based geopolymer with/without addition of heavy metals

3.4.1. SEM results

Fig. 11 shows the SEM images and energy-dispersive X-ray (EDX) spectra of the selected samples. The RET-based geopolymer exhibited a dense and compact microstructure, with some microcracks originating from compression testing and shrinkage (Fig. 11a). According to its EDX spectrum (Fig. 11b, spot 2), the geopolymer matrix mainly comprised O, Al, and Si, which indicated the formation of the –O–Si–O–Al–O– network. In addition, a particle was embedded in the geopolymer

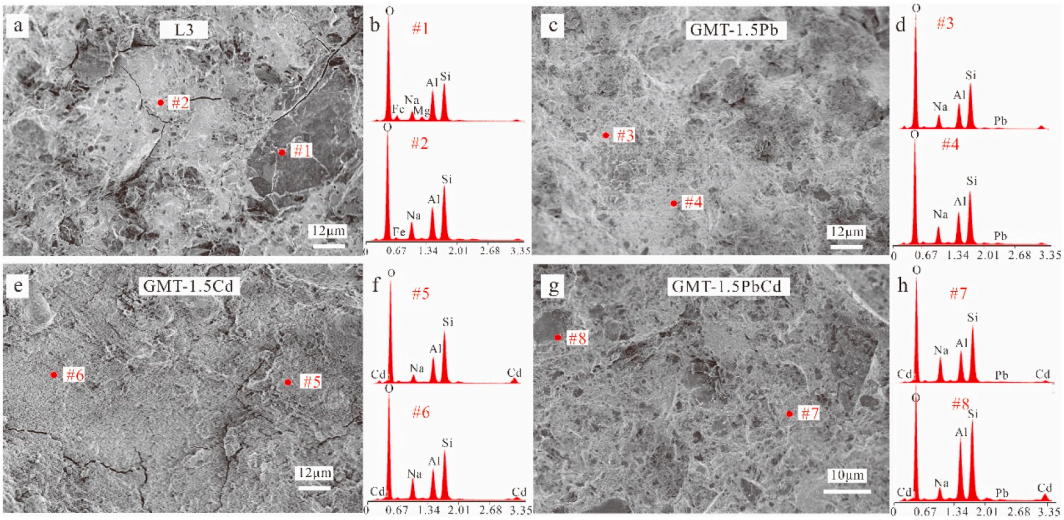

Fig. 11. (a), (c), (e), (g) scanning electron microscopy images and (b), (d), (f), (h) energy-dispersive X-ray spectra of selected spots of geopolymers with and without the addition of heavy metals.

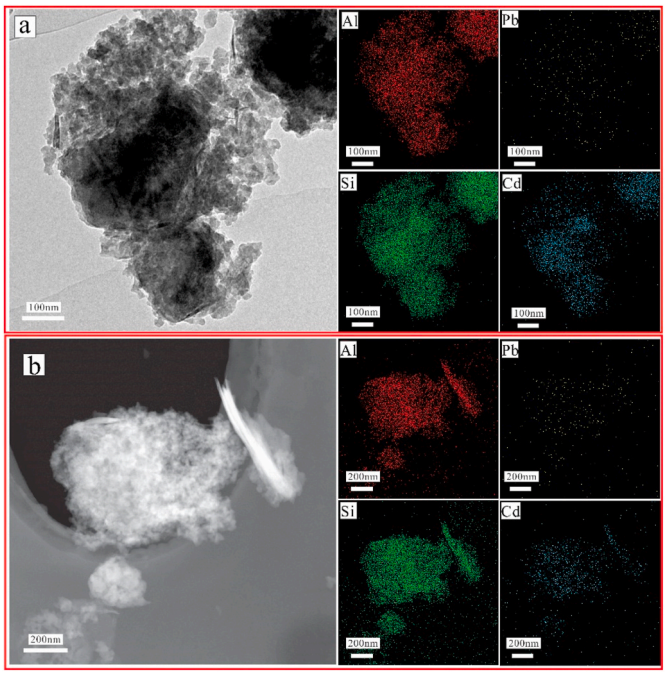

Fig. 12. (a) Transmission electron microscopy images with elemental mapping of RET-based geopolymers: (a) GMT-1.5PbCd and (b) GMT-1.5PbCd–F.

matrix, which mainly comprised Fe, Mg, Al, and Si (Fig. 11b, spot 1). This particle is expected to correspond to the unreacted minerals with low reactivity.

The geopolymer matrix became less compact after the addition of heavy metals, which responded to the reduced compressive strength. As discussed in Section 3.2.1, the addition of heavy metals consumed the alkaline solution, and thus, reduced the solution alkalinity, which inhibited the geopolymerization of $RET_{750°C}$. The EDX results displayed in Table 1 show the presence of two phases based on the Na/Al molar ratio (i.e., one phase with a Na/Al molar ratio near 1.0 and another for which the ratio is much lower than 1.0). As is well-known, Na^+ is required to balance the negative charges of $[AlO_4]$ units in the geopolymer network. Therefore, the phases with a Na/Al molar ratio close to 1.0 are attributable to the geopolymer (spots 3, 4, 6, and 7), while those with a lower Na/Al molar ratio are attributable to phases rich in unreacted minerals. The points with a Na/Al molar ratio near 1.0 included higher contents of heavy metals than the points with a low Na/Al molar ratio, which indicated that heavy metals were mainly immobilized in the geopolymer matrix.

3.4.2. *Transmission electron microscopy (TEM) results*

Fig. 12 and S3–S5 show the TEM images and EDX results of the selected samples. As seen, the geopolymer mainly comprised a gel agglomeration without a regular shape or morphology, because geopolymer is amorphous in nature. Unreacted quartz separated from the geopolymer was also observed in GMT-1.5 Pb (Fig. S4).

The TEM mapping of GMT-1.5PbCd presented in Fig. 11a shows that the Si and Al elements were distributed in the entire geopolymer matrix. In addition, Pb and Cd were evenly distributed in the geopolymer matrix, and were both positively correlated with Si and Al elements. This result clearly demonstrated that the heavy metals were homogeneously incorporated in the entire geopolymer matrix. Owing to the different atomic masses, the proportion of Cd was higher than that of Pb. In contrast, the unreacted minerals, such as quartz, exhibited little capacity for immobilization of heavy metals (Fig. S4). In the selected-area electron diffraction (SAED) image (inset of Figs. S3b and S5), the *d*-spacings shown in GMT-1.5Cd and GMT-1.5Cd–F can be attributed to the diffraction of the unreacted minerals, such as illite and microcline. No reflection corresponding to the crystal metal silicate (e.g., $PbSiO_3$ or $CdSiO_3$) could be found in the SAED patterns of the metal-containing geopolymers. This result further confirms that there was no formation of crystalline $PbSiO_3$ and $CdSiO_3$. According to Nikolić et al. [67], heavy metals mainly exist in the geopolymer matrix in the form of amorphous metal silicate or metal-incorporated aluminum-deficient aluminosilicate gel.

After leaching, the evident decrease in the content of Na^+ indicated the considerable exchange of Na^+ for H^+ (Table S2). Cd^{2+} and Pb^{2+} were still uniformly distributed in the geopolymeric matrix after leaching. The amounts of Pb^{2+} did not change substantially after the leaching test (Fig. 12b, Table S2), which demonstrated that the heavy metals were effectively immobilized. However, the amount of Cd^{2+} decreased to a certain extent, reflecting that Cd^{2+} was less effectively immobilized in the geopolymer matrix than Pb^{2+}. This result also agreed with the leaching results (Fig. 5).

3.5. *Mechanism of alkali-activation of RET and immobilization of heavy metals*

The above results demonstrated that the ion-adsorption type RET, which are potential starting materials for geopolymer preparation, contains halloysite, kaolinite, and other minerals rich in active Si and Al. In this study, the calcined RET, without the necessity of adding any other active additive (e.g., metakaolinite or activated silica), could be used to prepare geopolymer with high compressive strength. During the alkali activation, the minerals with high reactivity (e.g., kaolinite and halloysite) dissolved to form oligomers, followed by polycondensation to form a geopolymer with a three-dimensional network structure. The curing temperature, liquid/solid ratio, and concentration and modulus of sodium silicate affected the dissolution and polycondensation behaviors of RET-based geopolymers, which ultimately influenced their mechanical properties. In contrast, other minerals with low reactivity (e.g., quartz and microcline) did not participate in the geopolymerization and acted as inert fillers.

The above findings also indicate that the heavy metals could be largely immobilized in the geopolymer matrix without altering the structure of the RET-based geopolymer (Figs. 6 and 7). In previous studies [52,71], heavy metals were mainly immobilized using three mechanisms: Mechanism 1, where the hydrated Na^+ or K^+, which balanced the negative charge of tetrahedral $[AlO_4]$, was replaced by heavy metals; Mechanism 2, where the heavy metals reacted with the nonbridging oxygen (i.e., $Si–O^-$ and $Al–O^-$) of the geopolymer to form T–O–M (heavy metals) bonds; and Mechanism 3, where the heavy metals precipitated in the form of silicates, hydroxides, or carbonate under the alkaline medium. Based on the results of this study, the heavy metals were mainly immobilized in the RET-based geopolymer matrix through the formation of Si–O–M or Al–O–M bonds. The formation of such a chemical bond can substantially improve the stability of a heavy metal, leading to its immobilization [72]. However, the incorporation of heavy metals in the geopolymer matrix induced changes in the compositions of the RET-based geopolymer (Fig. 10), which altered its mechanical properties. Furthermore, a part of the heavy metal ions replaced Na^+ in the geopolymer matrix and were electrostatically attracted to the negatively charged $[AlO_4]^-$, thus balancing the partial charge of the geopolymer, as confirmed by the XPS results (Fig. 8). Such heavy metals might be more liable to leach out than to form chemical bonds during immersion in an acidic solution [66].

However, based on the XRD (Fig. 4) and SEAD results (insets of Fig. S3b, Fig. S5), no crystal containing Pb or Cd was observed in the geopolymers. Hence, there is no direct evidence regarding the formation of metal silicates, hydroxides, or carbonate after the immobilization of the heavy metals. This result was supported by those of previous studies, which concluded that the heavy metal was in the form of silicate glass or incorporated in the network instead of the crystal [5,10,67,72]. Besides, heavy metals cannot be incorporated or immobilized in impurities such

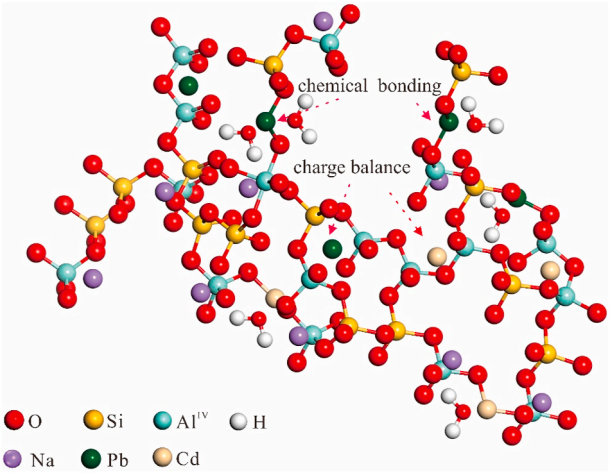

Fig. 13. Schematic diagram of immobilization forms of heavy metals in RET-based geopolymers.

as quartz. Therefore, as shown in Fig. 13, Mechanisms 1 and 2 form the main immobilization mechanism for heavy metals in the RET-based geopolymer matrix.

4. Conclusions

Ion-adsorption type rare earth tailing (RET) are a type of solid waste from mining activity that contains clay minerals with high geopolymerization reactivity, such as halloysite and kaolinite. In this study, the alkali activation of RET was conducted to prepare geopolymeric materials with a dense microstructure and desirable mechanical properties. The highest compressive strength of an RET-based geopolymer reached 28.5 MPa. In addition, this geopolymer exhibited high immobilization efficiency for Pb^{2+} and Cd^{2+}, which were incorporated and uniformly distributed in the geopolymer matrix. The immobilization efficiency of Pb^{2+} (above 99%) was higher than that of Cd^{2+} (92–96%). The heavy metals were effectively immobilized through two reactions: reaction of heavy metals and T (Si, Al)–O^- to form T–O–M bonds, and electrostatic attraction between metal cations and negatively charged $[AlO_4]^-$.

The above results demonstrate that ion-adsorption type RET are a promising candidate for preparing geopolymers with suitable performance. They suggest that the as-obtained geopolymer has a desirable capacity for immobilizing heavy metals (Pb^{2+} and Cd^{2+}), and exhibits suitable potential for reducing the environmental impact of RET and developing high-value-added products for the associated industries.

This study presents initial results of ion-adsorption type RET-based geopolymer with ability to immobilize Pb^{2+} and Cd^{2+}. Further research is needed to improve the understanding of its ability to immobilize other valence of heavy metals by static and dynamic leaching test, and investigation on related mechanism, as well as studying and improving other mechanical properties of this kind of geopolymer or geopolymer concrete.

Declaration of competing interest

The authors declare that they have no known competing financial interests or personal relationships that could have appeared to influence the work reported in this paper.

Data availability

Data will be made available on request.

Acknowledgements

Financial support by the National Special Support for High-Level Personnel, the National Natural Science Foundation of China (Grant Nos. 52161145405 and 41972045) are gratefully acknowledged. This is a contribution No. IS-3247 from GIGCAS.

Appendix A. Supplementary data

Supplementary data to this article can be found online at https://doi.org/10.1016/j.cemconcomp.2022.104768.

References

[1] W. Huo, Z. Zhu, W. Chen, J. Zhang, Z. Kang, S. Pu, Y. Wan, Effect of synthesis parameters on the development of unconfined compressive strength of recycled waste concrete powder-based geopolymers, Construct. Build. Mater. 292 (2021), 123264.
[2] A. Nazari, A. Bagheri, J.G. Sanjayan, M. Dao, C. Mallawa, P. Zannis, S. Zumbo, Thermal shock reactions of Ordinary Portland cement and geopolymer concrete: microstructural and mechanical investigation, Construct. Build. Mater. 196 (2019) 492–498.
[3] A.M. Aguirre-Guerrero, R.A. Robayo-Salazar, R.M. de Gutiérrez, A novel geopolymer application: coatings to protect reinforced concrete against corrosion, Appl. Clay Sci. 135 (2017) 437–446.
[4] C. Shi, B. Qu, J.L. Provis, Recent progress in low-carbon binders, Cement Concr. Res. 122 (2019) 227–250.
[5] F. Muhammad, X. Huang, S. Li, M. Xia, M. Zhang, Q. Liu, M.A. Shehzad Hassan, B. Jiao, L. Yu, D. Li, Strength evaluation by using polycarboxylate superplasticizer and solidification efficiency of Cr^{6+}, Pb^{2+} and Cd^{2+} in composite based geopolymer, J. Clean. Prod. 188 (2018) 807–815.
[6] Z. Ji, Y. Pei, Immobilization efficiency and mechanism of metal cations (Cd^{2+}, Pb^{2+} and Zn^{2+}) and anions (AsO_4^{3-} and $Cr_2O_7^{2-}$) in wastes-based geopolymer, J. Hazard Mater. 384 (2020), 121290.
[7] X. Guo, L. Zhang, J. Huang, H. Shi, Detoxification and solidification of heavy metal of chromium using fly ash-based geopolymer with chemical agents, Construct. Build. Mater. 151 (2017) 394–404.
[8] Z. Ji, Y. Pei, Bibliographic and visualized analysis of geopolymer research and its application in heavy metal immobilization: a review, J. Environ. Manag. 231 (2019) 256–267.
[9] W. Long, T. Ye, F. Xing, K.H. Khayat, Decalcification effect on stabilization/solidification performance of Pb-containing geopolymers, Cem. Concr. Compos. 114 (2020), 103803.
[10] Q. Wan, F. Rao, S. Song, C.A. Leon-Patino, Y. Ma, W. Yin, Consolidation of mine tailings through geopolymerization at ambient temperature, J. Am. Ceram. Soc. 102 (2018) 2451–2461.
[11] F. Demir, E.M. Derun, Modelling and optimization of gold mine tailings based geopolymer by using response surface method and its application in Pb^{2+} removal, J. Clean. Prod. 237 (2019), 117766.
[12] Y.H.M. Amran, R. Alyousef, H. Alabduljabbar, M. El-Zeadani, Clean production and properties of geopolymer concrete; A review, J. Clean. Prod. 251 (2020), 119679.
[13] B. Zhang, H. Guo, P. Yuan, L. Deng, D. Liu, Novel acid-based geopolymer synthesized from nanosized tubular halloysite: the role of precalcination temperature and phosphoric acid concentration, Cem. Concr. Compos. (2020), 103601.
[14] Q. Wang, H. Guo, T. Yu, P. Yuan, L. Deng, B. Zhang, Utilization of calcium carbide residue as solid alkali for preparing fly ash-based geopolymers: dependence of compressive strength and microstructure on calcium carbide residue, water content and curing temperature, Materials 15 (3) (2022) 973.
[15] J. Shekhovtsova, I. Zhernovsky, M. Kovtun, N. Kozhukhova, I. Zhernovskaya, E. Kearsley, Estimation of fly ash reactivity for use in alkali-activated cements - a step towards sustainable building material and waste utilization, J. Clean. Prod. 178 (2018) 22–33.
[16] X. Ge, X. Hu, C. Shi, The effect of different types of class F fly ashes on the mechanical properties of geopolymers cured at ambient environment, Cem. Concr. Compos. (2022), 104528.
[17] G. Gu, T. Ma, F. Chen, F. Xu, J. Zhang, Electromagnetic and mechanical properties of FA-GBFS geopolymer composite used for induction heating of airport pavement, Cem. Concr. Compos. 129 (2022), 104503.
[18] N. Belmokhtar, H. El Ayadi, M. Ammari, L. Ben Allal, Effect of structural and textural properties of a ceramic industrial sludge and kaolin on the hardened geopolymer properties, Appl. Clay Sci. 162 (2018) 1–9.
[19] N. Zhang, A. Hedayat, L. Figueroa, K.X. Steirer, H. Li, H.G. Bolaños Sosa, R. P. Huamani Bernal, N. Tupa, I.Y. Morales, R.S. Canahua Loza, Experimental studies on the durability and leaching properties of alkali-activated tailings subjected to different environmental conditions, Cem. Concr. Compos. (2022), 104531.
[20] M. Maksoud, A.M. Elgarahy, C. Farrell, A.H. Al-Muhtaseb, D.W. Rooney, A. I. Osman, Insight on water remediation application using magnetic nanomaterials and biosorbents, Coord. Chem. Rev. 403 (2020) 33.
[21] J.B. Yang, W.Y. Yang, F.S. Li, Y.C. Yang, Research and development of high-performance new microwave absorbers based on rare earth transition metal compounds: a review, J. Magn. Magn Mater. 497 (2020) 11.

[22] M. Yang, X. Liang, L. Ma, J. Huang, H. He, J. Zhu, Adsorption of REEs on kaolinite and halloysite: a link to the REE distribution on clays in the weathering crust of granite, Chem. Geol. 525 (2019) 210–217.
[23] Z. Deng, L. Qin, G. Wang, S. Luo, C. Peng, Q. Li, Metallogenic process of ion adsorption REE ore based on the occurrence regularity of La in kaolin, Ore Geol. Rev. 112 (2019), 103022.
[24] J. Kynicky, M.P. Smith, C. Xu, Diversity of rare earth deposits: the key example of China, Elements 8 (2012) 361–367.
[25] Y. Wang, H. Liang, Q. Chang, X. Zhang, J. Zhou, Separation of kaolinite from ion-adsorption rare earth tailings in southern China and iron removal treatment, J. Miner. Mater. Char. Eng. (2016) 40–47, 04.
[26] L. Kaizhong, L. Huiping, L. Fuguo, X. Yanfei, H. Yongmei, W. Chao, X. Haibo, Migration of natural radionuclides in the extraction process of the ion-adsorption type rare earths ore, Hydrometallurgy 171 (2017) 236–244.
[27] H. Lu, L. Cao, L. Yin, J. Yuan, Q. Zhao, Mineral-leaching chemical transport with runoff and sediment from severely eroded rare-earth tailings in southern China, Solid Earth Discussions 8 (2017) 845–855.
[28] Z. Gao, Q. Zhou, Contamination from rare earth ore strip mining and its impacts on resources and eco-environment, Chinese Journal of Ecology 30 (2011) 2915–2922 (in Chinese).
[29] W. Nie, R. Zhang, Z. He, J. Zhou, M. Wu, Z. Xu, R. Chi, H. Yang, Research progress on leaching technology and theory of weathered crust elution-deposited rare earth ore, Hydrometallurgy 193 (2020), 105295.
[30] J. Liu, F. Zha, L. Xu, B. Kang, C. Yang, W. Zhang, J. Zhang, Z. Liu, Zinc leachability in contaminated soil stabilized/solidified by cement-soda residue under freeze-thaw cycles, Appl. Clay Sci. 186 (2020), 105474.
[31] A.Z. Khalifa, Ö. Cizer, Y. Pontikes, A. Heath, P. Patureau, S.A. Bernal, A.T. M. Marsh, Advances in alkali-activation of clay minerals, Cement Concr. Res. 132 (2020), 106050.
[32] B. Zhang, H. Guo, L. Deng, W. Fan, T. Yu, Q. Wang, Undehydrated kaolinite as materials for the preparation of geopolymer through phosphoric acid-activation, Appl. Clay Sci. 199 (2020), 105887.
[33] S. Hu, L. Zhong, X. Yang, H. Bai, B. Ren, Y. Zhao, W. Zhang, X. Ju, H. Wen, S. Mao, R. Tao, C. Li, Synthesis of rare earth tailing-based geopolymer for efficiently immobilizing heavy metals, Construct. Build. Mater. 254 (2020), 119273.
[34] C. Luo, X. Luo, N. Zhou, Y. Zhang, Y. Deng, Status and Causes of Ecological Imbalance of Abandoned Rare-Earth Mine in South China, China Mining Magazine, 2014, pp. 65–70 (in Chinese).
[35] Y. He, B. Li, K. Zhang, Z. Li, Y. Chen, W. Ye, Experimental and numerical study on heavy metal contaminant migration and retention behavior of engineered barrier in tailings pond, Environ. Pollut. 252 (2019) 1010–1018.
[36] L. Yun-Ming, H. Cheng-Yong, M.M. Al Bakri, K. Hussin, Structure and properties of clay-based geopolymer cements: a review, Prog. Mater. Sci. 83 (2016) 595–629.
[37] R. Firdous, D. Stephan, Effect of silica modulus on the geopolymerization activity of natural pozzolans, Construct. Build. Mater. 219 (2019) 31–43.
[38] D. Bondar, C.J. Lynsdale, N.B. Milestone, N. Hassani, A.A. Ramezanianpour, Effect of type, form, and dosage of activators on strength of alkali-activated natural pozzolans, Cem. Concr. Compos. 33 (2011) 251–260.
[39] A. Gharzouni, E. Joussein, B. Samet, S. Baklouti, S. Pronier, I. Sobrados, J. Sanz, S. Rossignol, The effect of an activation solution with siliceous species on the chemical reactivity and mechanical properties of geopolymers, J. Sol. Gel Sci. Technol. 73 (2015) 250–259.
[40] B. Zhang, P. Yuan, H. Guo, L. Deng, Y. Li, L. Li, Q. Wang, D. Liu, Effect of curing conditions on the microstructure and mechanical performance of geopolymers derived from nanosized tubular halloysite, Construct. Build. Mater. 268 (2021), 121186.
[41] T. Bai, Z. Song, H. Wang, Y. Wu, W. Huang, Performance evaluation of metakaolin geopolymer modified by different solid wastes, J. Clean. Prod. 226 (2019) 114–121.
[42] Z. Zhang, H. Wang, X. Yao, Y. Zhu, Effects of halloysite in kaolin on the formation and properties of geopolymers, Cem. Concr. Compos. 34 (5) (2012) 709–715.
[43] X. Chen, Y. Guo, S. Ding, H. Zhang, F. Xia, J. Wang, M. Zhou, Utilization of red mud in geopolymer-based pervious concrete with function of adsorption of heavy metal ions, J. Clean. Prod. 207 (2019) 789–800.
[44] H. Wang, H. Li, F. Yan, Synthesis and mechanical properties of metakaolinite-based geopolymer, Colloids Surf., A 268 (1) (2005) 1–6.
[45] Z. Zhang, Y. Xiao, Z. Huajun, C. Yue, Role of water in the synthesis of calcined kaolin-based geopolymer, Appl. Clay Sci. 43 (2009) 218–223.
[46] S. Alonso, A. Palomo, Alkaline activation of metakaolin and calcium hydroxide mixtures: influence of temperature, activator concentration and solids ratio, Mater. Lett. 47 (1) (2001) 55–62.
[47] J. He, Y. Jie, J. Zhang, Y. Yu, G. Zhang, Synthesis and characterization of red mud and rice husk ash-based geopolymer composites, Cem. Concr. Compos. 37 (2013) 108–118.
[48] X. Yao, Z. Zhang, H. Zhu, Y. Chen, Geopolymerization process of alkali–metakaolinite characterized by isothermal calorimetry, Thermochim. Acta 493 (1) (2009) 49–54.
[49] S. Lee, A. van Riessen, C. Chon, N. Kang, H. Jou, Y. Kim, Impact of activator type on the immobilisation of lead in fly ash-based geopolymer, J. Hazard Mater. 305 (2016) 59–66.
[50] H. Wei, Q. Nie, B. Huang, S. Xiang, H. Qiang, Mechanical and microstructural characterization of geopolymers derived from red mud and fly ashes, J. Clean. Prod. 186 (2018) 199–806.
[51] H. Xu, J.S.J.V. Deventer, The geopolymerisation of alumino-silicate minerals, Int. J. Miner. Process. 59 (2000) 247–266.
[52] B.I. El-Eswed, O.M. Aldagag, F.I. Khalili, Efficiency and mechanism of stabilization/solidification of Pb(II), Cd(II), Cu(II), Th(IV) and U(VI) in metakaolin based geopolymers, Appl. Clay Sci. 140 (2017) 148–156.
[53] D. Hou, J. Zhang, W. Pan, Y. Zhang, Z. Zhang, Nanoscale mechanism of ions immobilized by the geopolymer: a molecular dynamics study, J. Nucl. Mater. 528 (2020), 151841.
[54] W. Qian, R. Feng, S. Song, M.E. Ricardo, X. Xie, T. Xiong, Chemical forms of lead immobilization in alkali-activated binders based on mine tailings, Cem. Concr. Compos. 92 (2018) 198–204.
[55] Z.Y. He, R. Zhang, W.R. Nie, Z.Y. Zhang, R. Chi, Z.G. Xu, M. Wu, J. Qu, Leaching process and mechanism of weathered crust elution-deposited rare earth ore, Mining Metall. Explor. 36 (2019) 1021–1031.
[56] J. Madejová, P. Komadel, Baseline studies of the clay minerals society source clays, Clay Clay Miner. 49 (5) (2001) 372–373.
[57] E. Kränzlein, J. Harmel, H. Pöllmann, W. Krcmar, Influence of the Si/Al ratio in geopolymers on the stability against acidic attack and the immobilization of Pb^{2+} and Zn^{2+}, Construct. Build. Mater. 227 (2019), 116634.
[58] Y. Wang, F. Han, J. Mu, Solidification/stabilization mechanism of Pb(II), Cd(II), Mn(II) and Cr(III) in fly ash based geopolymers, Construct. Build. Mater. 160 (2018) 818–827.
[59] Q. Yu, S. Li, H. Li, X. Chai, X. Bi, J. Liu, T. Ohnuki, Synthesis and characterization of Mn-slag based geopolymer for immobilization of Co, J. Clean. Prod. 234 (2019) 97–104.
[60] Q. Tian, B. Guo, K. Sasaki, Immobilization mechanism of Se oxyanions in geopolymer: effects of alkaline activators and calcined hydrotalcite additive, J. Hazard Mater. 387 (2020), 121994.
[61] X. Guo, J. Huang, Effects of Cr^{3+}, Cu^{2+}, and Pb^{2+} on fly ash based geopolymer, J. Wuhan Univ Technol. 34 (2019) 851–857.
[62] T. Lan, P. Li, F.U. Rehman, X. Li, W. Yang, S. Guo, Efficient adsorption of Cd^{2+} from aqueous solution using metakaolin geopolymers, Environ. Sci. Pollut. Res. 26 (2019) 33555–33567.
[63] A.M. Abdel-Mageed, K. Wiese, M. Parlinska-Wojtan, J. Rabeah, A. Bruckner, R. J. Behm, Encapsulation of Ru nanoparticles: modifying the reactivity toward CO and CO_2 methanation on highly active Ru/TiO_2 catalysts, Appl. Catal. B Environ. 270 (2020) 14.
[64] M. Jin, Z. Zheng, Y. Sun, L. Chen, Z. Jin, Resistance of metakaolin-MSWI fly ash based geopolymer to acid and alkaline environments, J. Non-Cryst. Solids 450 (2016) 116–122.
[65] Z. Ji, Y. Pei, Geopolymers produced from drinking water treatment residue and bottom ash for the immobilization of heavy metals, Chemosphere 225 (2019) 579–587.
[66] B. Walkley, X. Ke, O.H. Hussein, S.A. Bernal, J.L. Provis, Incorporation of strontium and calcium in geopolymer gels, J. Hazard Mater. 382 (2020), 121015.
[67] V. Nikolić, M. Komljenović, N. Džunuzović, Z. Miladinović, The influence of Pb addition on the properties of fly ash-based geopolymers, J. Hazard Mater. 350 (2018) 98–107.
[68] Z. Baščarević, M. Komljenović, Z. Miladinović, V. Nikolić, N. Marjanović, Z. Žujović, R. Petrović, Effects of the concentrated NH4NO3 solution on mechanical properties and structure of the fly ash based geopolymers, Construct. Build. Mater. 41 (2013) 570–579.
[69] C. Ruiz-Santaquiteria, J. Skibsted, A. Fernández-Jiménez, A. Palomo, Alkaline solution/binder ratio as a determining factor in the alkaline activation of aluminosilicates, Cem, Concr. Res. 42 (2012) 1242–1251.
[70] Violeta, Miroslav Nikolić, Nataša Komljenović, Tijana Džunuzović, Zoran Ivanović, Immobilization of hexavalent chromium by fly ash-based geopolymers, Compos Part B 112 (2017) 213–223.
[71] B.I. El-eswed, Chemical evaluation of immobilization of wastes containing Pb, Cd, Cu and Zn in alkali-activated materials: a critical review, J. Environ. Chem. Eng. 8 (5) (2020), 104194.
[72] J. Sato, K. Shiota, M. Takaoka, Stabilization of lead with amorphous solids synthesized from aluminosilicate gel, J. Hazard Mater. 385 (2020), 121109.